Journal of Energy Storage 32 (2020) 101834

Contents lists available at ScienceDirect

Journal of Energy Storage

journal homepage: www.elsevier.com/locate/est

# Entropy generation and natural convection flow of a suspension containing nano-encapsulated phase change particles in a semi-annular cavity

Mehdi Ghalambaz[a,b], S.A.M. Mehryan[c], Masoud Mozaffari[d], Ahmad Hajjar[e], Mohamad El Kadri[f], Nesrine Rachedi[g], Mikhail Sheremet[h], Obai Younis[i,j], Sohail Nadeem[k,l,*]

[a] Institute of Research and Development, Duy Tan University, Da Nang 550000, Vietnam
[b] Faculty of Electrical – Electronic Engineering, Duy Tan University, Da Nang 550000, Vietnam
[c] Young Researchers and Elite Club, Yasooj Branch, Islamic Azad University, Yasooj, Iran
[d] Department of Mechanical Engineering, Najafabad Branch, Islamic Azad University, Najafabad, Iran
[e] ECAM Lyon, LabECAM, Université de Lyon, Lyon, France
[f] Centre Scientifique et Technique du Bâtiment, Nantes, France
[g] Laboratoire de Génie des Procédés Chimiques, Université Ferhat Abbas Sétif-1, Sétif 19000, Algeria
[h] Laboratory on Convective Heat and Mass Transfer, Tomsk State University, Tomsk, Russian Federation
[i] Department of Mechanical Engineering, College of Engineering at Wadi Addwaser, Prince Sattam Bin Abdulaziz University, KSA
[j] Department of Mechanical Engineering, Faculty of Engineering, University of Khartoum, Sudan
[k] Mathematics and Its Applications in Life Sciences Research Group, Ton Duc Thang University, Ho Chi Minh City, Vietnam
[l] Faculty of Mathematics and Statistics, Ton Duc Thang University, Ho Chi Minh City, Vietnam

ARTICLE INFO

*Keywords:*
Entropy generation
Nano-Encapsulated Phase Change Materials (NEPCM)
NEPCM-suspension
Energy Storage

ABSTRACT

The natural phase change convection of a new type of hybrid nanofluids, suspensions of Nano-Encapsulated Phase Change Materials (NEPCM), was addressed in a semi-annular inclined enclosure. The nanoparticles consist of a polymer shell and a nonadecane shell, in which the nonadecane core can change phase at its melting temperature and absorb/release a significant quantity of latent heat. The NEPCM-suspension circulates in the enclosure due to the natural convection, and the NEPCM particles contribute to heat transfer by phase change. The equations governing the movement and heat transfer of the suspension and nanoparticles were inserted in the form of partial differential equations. The finite element method was used to numerically solve the equations. Then, the entropy generation of NEPCM suspension in the attendance of the phase change was examined. The influence of the fusion temperature and volume fraction of nanoparticles, Stefan number, Rayleigh number, and inclination angle of enclosure on the thermal behavior and entropy generation of the suspension was explored. The results showed that the contribution of phase change core of nanoparticles was significant, and the heat transfer was enhanced by the presence of NEPCM particles. The fusion temperature of particles controls the Bejan number (entropy generation) behavior of the NEPCM suspension. There is an optimum phase change temperature for nanoparticles, which results in maximum heat transfer. For a horizontal enclosure, the optimum fusion temperature is the average temperature of the active walls. This optimum phase change temperature is a function of the tilting angle of the enclosure.

## 1. Introduction

Phase change materials (PCM) are used to store and release heat when the phase transition occurs [1]. They undergo a solid-liquid phase alteration for a relatively small temperature difference. The PCMs are used in several fields, as building energy conservation [2], heat exchangers [3], electronic devices [4], and other fields. Recently, this technology was used in the devices made of materials, which have different thermal expansion coefficients and risk of temperature gradients. In such states, the encapsulation of the PCM is employed in order to control the device temperature better.

The PCMs are encapsulated in shell structures and, when at minimum, one dimension of these capsules is nanometer size, the term Nano-Encapsulated Phase Change Materials (NEPCMs) could be used. The Nano-enhanced Phase Change Materials (NePCMs) are another type of PCMs, in which the solid nanoparticles are dispersed in a PCM to enhance its thermal conductivity. Hence, in the use of the abbreviation, there should be a distinction between these two subjects by using small

* Corresponding author.
*E-mail addresses:* mehdighalambaz@duytan.edu.vn (M. Ghalambaz), sohail.nadeem@tdtu.edu.vn (S. Nadeem).

https://doi.org/10.1016/j.est.2020.101834
Received 6 August 2020; Received in revised form 26 August 2020; Accepted 30 August 2020
Available online 14 September 2020

**Nomenclatures**

*Latin symbols*

| | |
|---|---|
| AR | Aspect ratio |
| Be | Bejan number |
| $C_p$ | Specific heat at constant pressure |
| Cr | Ratio of heat capacity of the suspension |
| f | Non-dimensional fusion function |
| g | Gravity |
| H | Non-dimensionalization characteristic length |
| k | Coefficient of the thermal conductivity |
| Nc | Suspension conductivity number |
| $Nu_a$ | Average Nusselt number |
| $N\nu$ | Suspension dynamic viscosity number |
| Pr | Prandtl number |
| Ra | Rayleigh number |
| $r_i$ | Radius of inner cylinder |
| $r_o$ | Radius of outer cylinder |
| $R_r$ | Radii ratio |
| S | Entropy |
| Ste | Stefan number |
| T | Temperature |
| u | x-velocity component |
| U | X-non-dimensional velocity |
| v | y-velocity component |
| V | Y-non-dimensional velocity |
| x, y | Coordinate components |
| X, Y | Non-dimensional coordinate |

*Greek symbols*

| | |
|---|---|
| α | Coefficient of thermal diffusivity |
| β | Thermal volume expansion coefficient |
| δ | Non-dimensional melting interval |
| θ | Non-dimensional fusion temperature |
| λ | Sensible heat capacity ratio of the suspension |
| μ | Fluid dynamic viscosity |
| ρ | Density |
| ϕ | Volume fraction of particles |
| ψ | Dimensional stream function |
| Ψ | Non-dimensional stream function |
| ω | Inclination angle |

*Subscripts*

| | |
|---|---|
| b | Bulk properties of the suspension, base fluid |
| c | Cold wall |
| co | NEPCM core |
| f | Fusion property |
| fu | The phase change |
| h | Hot wall |
| M | Maximum |
| p | NEPCM particles |
| sh | NEPCM shell |
| T | Thermal |
| TO | Total |
| V | Viscous |

and capital letters. The NePCMs have been reviewed in [5, 6], and various aspects of enhanced phase change materials have also been investigated in [2, 7-9].

Considering NEPCMs, several PCMs are used for encapsulation, such as the n-octadecane, n-nonadecane, n-tetradecane, and n-octacosane. The shell is made of polymers such as polymer-$SiO_2$ [10]. The NEPCM are synthesized by different techniques such as spray drying [11], layer by layer assembly [12, 13], and interfacial polymerization [14, 15]. The polymerization method is the most used in industry due to its feasibility and robustness [16]. Since the use of polymeric materials as shell in the NEPCM leads to the issue of low thermal conductivity, the inorganic materials such as titanium oxide and silica were studied in order to promote the thermal properties of nano encapsulated PCMs [17, 18]. The silica showed better thermal properties among inorganic materials [19]. Fu et al. [20] synthesized a NEPCM slurry using n-tetradecane and polystyrene-silica shell composite for low-temperature energy storage applications. Ushak et al. [21] proposed encapsulated particles with a high fusion enthalpy of 116.2 kJ $kg^{-1}$. However, the size of particles was large (500 μm). So synthesis of a slurry with such particle's sizes would increase the solution instability and sedimentation.

Suspensions of NEPCM dispersed in base fluids represent a new class of nanofluids in which the nanoparticles store/release latent heat. The literature survey indicates that various aspects of convective heat transfer of the simple nanofluids with no phase change have been investigated in cavities. For instance, Rachad et al. [22] studied the effect of a heat source location and size on the heat transfer of Cu-water nanofluids in a tilted porous cavity. They concluded that a rise in the concentration of nanoparticles could deteriorate the convective heat transfer in the cavity. Sheikholeslami et al. [23] analyzed the convective heat transfer of MWCNT-$Fe_3O_4$/$H_2O$ hybrid nanofluid in a circular enclosure in the presence of two heated cylinders. The results showed heat transfer enhancement by using hybrid nanoparticles. The thermal performance and advancement of hybrid nanofluids have been addressed in [24, 25]. Alsabery et al. [26] studied the conjugate mixed convection heat transfer of nanofluids in a lid-driven enclosure. They used a two-phase model for the nanofluid and investigated the concentration distribution of the nanoparticles in the cavity. The simulation data shows that the temperature gradient moves the nanoparticles away from hot walls. In another study, Alsabery et al. [27] examined the transient free convection of $Al_2O_3$-water nanofluids in a porous cavity. They focused on the impact of the porosity, Darcy number, and concentration of nanoparticles on the heat transfer rate (Average Nusselt number). It was found that Nusselt number is a rising function of Darcy number; however, the increase of porosity could promote the average Nusselt number only when the Darcy number was high. Thus, using nanoparticles could be advantageous at high porosity and high Darcy number designs. The convection heat transfer of nanofluids have been investigated considering tall cavities [28], open cavities [29], porous cavities [30], solar collectors [31], and non-Newtonian effects [32].

As seen, the convective heat transfer of simple nanofluids and hybrid nanofluids has received a notable amount of attention. However, the nanofluids with encapsulated phase change nanoparticles are a new subject, and only a few publications have addressed their convective heat transfer behavior. The majority of works regarding suspensions of encapsulated particles deal with forced convection. For example, Ho et al. [33] examined the laminar forced convection flow of nanofluids and encapsulated phase change material suspensions in minichannel heat sinks. They found that employing the encapsulated particle could change the heat transfer behavior of the working liquid (water). The advantage of using encapsulated particles was under the significant influence of the flow rate and heating location in the channel.

Seyf et al. [34] carried out a numerical solution to examine the heat transfer advantage of employing a NEPCM-slurry in the forced convection heat transfer over an isothermal square block. They found that the use of NEPCM slurry significantly augments the heat transfer compare to the base fluid. The rise of the nanoparticle concentration and Reynolds numbers increase the benefit of employing the slurry.

The free convection heat transfer of NEPCM-suspensions has been explored in some of the recent publications. Ghalambaz et al. [35] studied the free convection flow of a NEPCM suspension in a square enclosure. There was zero heat flux at the horizontal walls, while the vertical walls were at different constant temperatures, in which the left wall was warmer than the right wall. They found that the particles' fusion temperature is a key parameter in the heat transfer. Using the phase change particles was most advantageous when the non-dimensional fusion temperature was between 0.25 and 0.75. In another investigation, Galamabaz et al. [36] modeled the free-convection transfer of a suspension involving NEPCMs in a porous medium. They concluded that the augment of porosity could be advantageous only when the volumetric concentration of the particles is higher than 3%.

Since the temperature of the walls can fluctuate in practice, Hajjar et al. [37] studied the free convection of a NEPCMs-suspension in an enclosure. There was a prescribed time-periodic temperature at the heated wall. The simulations showed that the higher concentration of phase change particles, the better the heat transfer rate. These studies showed that the increase of the volume fraction of the NEPCM enhances the heat transfer. As seen, using phase change particles is beneficial in most cases; however, at some limits, a further increase could raise the viscous forces or reduce the sensible heat capacity of the working liquid and affect the heat transfer. Later, Mehryan et al. [38] analyzed the free convection heat transfer of NEPCMs-suspensions in an eccentric annulus.

Zadeh et al. [39] analyzed the irreversibility behavior of a NEPCM-suspension in a square enclosure with thick walls. The cavity was filled with a porous medium and saturated with the suspension. The irreversibility analysis showed that a fusion temperature equal to the average temperature of the cavity-walls could yield to minimum irreversibilities and maximum heat transfer rate.

The literature review indicates that the subject of hybrid nanofluids made of NEPCM particles is a new topic, and only a few publications have considered the flow and heat transfer of such advanced fluids. The impact of an enclosure-shape and the variation of the gravity vector on the heat transfer behavior of NEPCM-suspensions is not clear, yet. Thus, the present work aims to investigate the natural convection heat transfer and entropy generation of NEPCM-suspensions in a semi-annular inclined enclosure for the first time.

## 2. Mathematical model

### 2.1. Physical model

A two-dimensional semi-annular cavity full of a suspension of the nano-encapsulated phase change particles and water is considered as the problem physics, as exhibited in Fig. 1. In addition, $\omega$ is the inclination angle of the semi-annular cavity.

As denoted in Fig. 1, the internal cylinder, mounted at ($r_o \cos(\omega)$, $r_o \sin(\omega)$), is maintained at a hot temperature of $T_h$. The outer wall is held at a cold isothermal temperature of $T_c$. Here, $R_r$ is the radii ratio, i.e. $r_o/r_i$. The shell and core of the nanoparticles are respectively polyurethane (PU) and nonadecane.

There are no thermal and hydrodynamic slips between the uniformly dispersed PU- nonadecane particles and water. The thermophysical components of the suspension are given in Table 1. In addition, the latent heat of the PCM material is 211 kJ/kg at a fusion temperature of 32 °C [40].

### 2.2. The mathematical formulation

Although the overall density of the suspension is constant, the effect of density variations on the buoyancy force was modeled by the Boussinesq approximation. Also, the heat generated in the suspension due to the shear forces, i.e., viscous dissipation, was neglected. The equations of hydrodynamic and thermal behavior of a laminar, Newtonian and incompressible uniform-suspension of nanoparticles have been listed below considering the foregoing assumptions:

Conservation of mass [35]:

$$\frac{\partial u}{\partial x} + \frac{\partial v}{\partial y} = 0 \tag{1}$$

Momentum equation for $x$ and $y$ directions [35, 41]:

$$\rho_b\left(u\frac{\partial u}{\partial x} + v\frac{\partial u}{\partial y}\right) = -\frac{\partial p}{\partial x} + \mu_b\left(\frac{\partial^2 u}{\partial x^2} + \frac{\partial^2 u}{\partial y^2}\right) + \rho_b g\beta_b(T - T_c)\sin(\omega) \tag{2-a}$$

$$\rho_b\left(u\frac{\partial v}{\partial x} + v\frac{\partial v}{\partial y}\right) = -\frac{\partial p}{\partial y} + \mu_b\left(\frac{\partial^2 v}{\partial x^2} + \frac{\partial^2 v}{\partial y^2}\right) + \rho_b g\beta_b(T - T_c)\cos(\omega) \tag{2-b}$$

Conservation of energy [35]:

$$(\rho C_p)_b\left(u\frac{\partial T}{\partial x} + v\frac{\partial T}{\partial y}\right) = k_b\left(\frac{\partial^2 T}{\partial x^2} + \frac{\partial^2 T}{\partial y^2}\right) \tag{3}$$

Here, $u$ and $v$ of the above equations are the components of the velocity vector along the $x$ and $y$ directions. ρ is the density, $p$ is the pressure, $\mu$ is the dynamic viscosity, $\beta$ is the thermal volume expansion, g is the gravity acceleration, $T$ is temperature, $k$ is the thermal conductivity, $C_p$ is the heat capacity. The subscript $b$ of equations (2-a), (2-b), and (3) denotes the bulk properties of the suspension. The boundary conditions are written according to the problem physics as:

$$\begin{aligned}
&\forall\, x, y | (x - r_o\cos(\omega))^2 + (y - r_o\sin(\omega))^2 = r_i^2 \Rightarrow u = v = 0,\ \mathrm{T} = \mathrm{T}_h\\
&\forall\, x, y | (x - r_o\cos(\omega))^2 + (y - r_o\sin(\omega))^2 = r_o^2 \Rightarrow u = v = 0,\ \mathrm{T} = \mathrm{T}_c\\
&\forall\, x, y \left| \begin{array}{l} 0 \le x \le (r_o - r_i)\cos(\omega),\ 0 \le y \le (r_o - r_i)\sin(\omega) \\ \quad \Rightarrow u = v = 0,\ \frac{\partial T}{\partial n} = 0 \\ (r_o + r_i)\cos(\omega) \le x \le 2r_o\cos(\omega), \\ (r_o + r_i)\cos(\omega) \le y \le 2r_o\sin(\omega) \end{array} \right. \Rightarrow u = v = 0,\ \frac{\partial T}{\partial n} = 0
\end{aligned} \tag{4}$$

### 2.3. Bulk properties of the suspension

The density of the suspension is written as a weighted function of the host fluid and NEPCM dispersed particles [42]:

$$\rho_b = (1 - \phi)\rho_f + \phi\rho_p \tag{5}$$

The $p$ and $f$ subscripts denote NEPCM particles and the base fluid, respectively. The density of NEPCM particles is evaluated as follows [43]:

$$\rho_p = \frac{(1 + \iota)\rho_{co}\rho_{sh}}{\rho_{sh} + \iota\rho_{co}} \tag{6}$$

$\rho_{sh}$ is the density of the shell, and $\rho_{co}$ is the density of the core of NEPCM particles. $\iota$ is the core-shell weight ratio as $\iota$~0.447 [40].

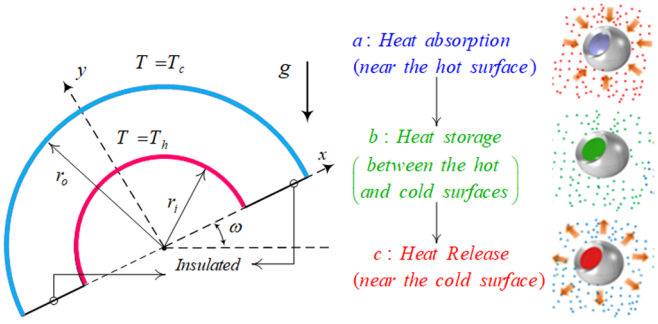


**Fig. 1.** Physical model and geometrical specifications.

**Table 1**
Thermophysical values of the core, shell, and water [38].

| | $\mu$ (kg/m. s) | $\beta$ ($K^{-1}$) | k (W/m.K) | $\rho$ ($Kg/m^3$) | $C_p$ (KJ/Kg.K) |
|---|---|---|---|---|---|
| Host fluid | $8.9 \times 10^{-4}$ | $21 \times 10^{-5}$ | 0.613 | 997.1 | 4179 |
| PU | — | $17.28 \times 10^{-5}$ | | 786 | 1317.7 |
| Nonadecane | — | | | 721 | 2037 |

Besides, the core's density was adopted as the average of solid-liquid phases. The specific heat capacity of the liquid-particles was introduced as [44]:

$$C_{p,b} = \frac{(1-\phi)\rho_f C_{p,f} + \phi\rho_p C_{p,p,eff}}{\rho_b} \tag{7}$$

In the case of no phase change, $C_{p,\ p,\ eff}$ is identical to the specific heat capacity of the NEPCM particle and can be calculated by the following formula:

$$C_{p,p} = \frac{(C_{p,co} + \iota C_{p,sh})\rho_{co}\rho_{sh}}{(\rho_{sh} + \iota\rho_{co})\rho_p} \tag{8}$$

The average of the fluid and solid heat capacities was considered as the specific heat capacity of the core of encapsulated nanoparticles. Since the nanoparticles' core undergoes a phase change, the specific heat capacity of the nanoparticles involves the latent heat of the change phase. The effective specific heat capacity can be modeled using the sinusoidal profile as the following [35]:

$$C_{p,p,eff} = C_{p,p} + \left\{\frac{\pi}{2}\cdot\left(\frac{h_{sf}}{T_{Mr}} - C_{p,p}\right)\cdot\sin\left(\pi\frac{T - T_{fu} + T_{Mr}/2}{T_{Mr}}\right)\right\}\gamma$$
$$\gamma = \begin{cases} 0 & T < T_{fu} - T_{Mr}/2 \\ 1 & T_{fu} - T_{Mr}/2 < T < T_{fu} + T_{Mr}/2 \\ 0 & T > T_{fu} + T_{Mr}/2 \end{cases} \tag{9}$$

$T_{Mr}$ is the temperature interval. Indeed, this temperature bond prevents the gradient discontinuities in the heat equation (Eq. (3)).

The thermal volume expansion coefficient of the suspension is written as [45]:

$$\beta_b = (1-\phi)\beta_f + \phi\beta_p \tag{10}$$

The two main mechanisms of entropy production, which are the viscosity and temperature gradient, are taken into account [46].

$$s_{TO} = s_T + s_V = \frac{k_b}{T_0^2}\left[\left(\frac{\partial T}{\partial x}\right)^2 + \left(\frac{\partial T}{\partial y}\right)^2\right] + \frac{\mu_b}{T_0}\left(2\left(\left(\frac{\partial u}{\partial x}\right)^2 + \left(\frac{\partial v}{\partial y}\right)^2\right) + \left(\frac{\partial u}{\partial y} + \frac{\partial v}{\partial x}\right)^2\right) \tag{11}$$

In above, $s_T$ and $s_V$ stands for the entropy generations due to the fluid friction and temperature gradients.

### 2.4. Non-dimensional equations

The following dimensionless variables are introduced and plugged into Eqs. (1)-(3):

$$X = \frac{x}{H},\ Y = \frac{y}{H},\ R_i = \frac{r_i}{H},\ R_o = \frac{r_o}{H},\ U = \frac{uH}{\alpha_f},\ V = \frac{vH}{\alpha_f},\ P = \frac{pH^2}{\rho_f\alpha_f^2},$$
$$\theta = \frac{T - T_c}{\Delta T} \tag{12}$$

where $H = r_o - r_i$and$\Delta T = T_h - T_c$. Hence, we then have:

$$\frac{\partial U}{\partial X} + \frac{\partial V}{\partial Y} = 0 \tag{13}$$

$$\left(\frac{\rho_b}{\rho_f}\right)\left(U\frac{\partial U}{\partial X} + V\frac{\partial U}{\partial Y}\right) = -\frac{\partial P}{\partial X} + Pr\left(\frac{\mu_b}{\mu_f}\right)\left(\frac{\partial^2 U}{\partial X^2} + \frac{\partial^2 U}{\partial Y^2}\right) + RaPr\left(\frac{\rho_b}{\rho_f}\right)\left(\frac{\beta_b}{\beta_f}\right)\theta\sin(\omega) \tag{14}$$

$$\left(\frac{\rho_b}{\rho_f}\right)\left(U\frac{\partial V}{\partial X} + V\frac{\partial V}{\partial Y}\right) = -\frac{\partial P}{\partial Y} + Pr\left(\frac{\mu_b}{\mu_f}\right)\left(\frac{\partial^2 V}{\partial X^2} + \frac{\partial^2 V}{\partial Y^2}\right) + RaPr\left(\frac{\rho_b}{\rho_f}\right)\left(\frac{\beta_b}{\beta_f}\right)\theta\cos(\omega) \tag{15}$$

The non-dimensional parameters, *Ra* and *Pr* numbers, are

$$Ra = \frac{g\rho_f\beta_f\Delta T H^3}{\alpha_f\mu_f},\ Pr = \frac{\mu_f}{\rho_f\alpha_f} \tag{16}$$

Also,

$$\left(\frac{\rho_b}{\rho_f}\right) = (1-\phi) + \phi\left(\frac{\rho_p}{\rho_f}\right),\quad \left(\frac{\beta_b}{\beta_f}\right) = (1-\phi) + \phi\left(\frac{\beta_p}{\beta_f}\right) \tag{17}$$

The volume difference between the liquid and particles' volume expansions was neglected, and hence, $\beta_b/\beta_f \sim 1$ [35, 39].

$$Cr\left(U\frac{\partial\theta}{\partial X} + V\frac{\partial\theta}{\partial Y}\right) = \left(\frac{k_b}{k_f}\right)\left(\frac{\partial^2\theta}{\partial X^2} + \frac{\partial^2\theta}{\partial Y^2}\right) \tag{18}$$

where

$$Cr = \frac{(\rho C_p)_b}{(\rho C_p)_f} = (1-\phi) + \phi\lambda + \frac{\phi}{\delta\ Ste}f \tag{19}$$

The parameter of *Cr* stands for a characteristic's indicator indicating the local heat capacity, including the latent heat of fusion. In addition, the sensible heat capacity ratio ($\lambda$), the scaled phase change bond ($\delta$), and the Stefan number (*Ste*) are computed as:

$$\lambda = \frac{(C_{p,co} + \iota C_{p,sh})\rho_{co}\rho_{sh}}{(\rho C_p)_f(\rho_{sh} + \iota\rho_{co})},\ \delta = \frac{T_{Mr}}{\Delta T},\ Ste = \frac{(\rho C_p)_f\Delta T(\rho_{sh} + \iota\rho_{co})}{\alpha_f(h_{sf}\rho_{co}\rho_{sh})} \tag{20}$$

In Eq. (19), $f$ is the dimensionless fusion function, introduced by:

$$f = \frac{\pi}{2}\sin\left(\frac{\pi}{\delta}(\theta - \theta_{fu} + \delta/2)\right)\sigma$$
$$\sigma = \begin{cases} 0 & \theta < \theta_{fu} - \delta/2 \\ 1 & \theta_{fu} - \frac{\delta}{2} < \theta < \theta_{fu} + \delta/2 \\ 0 & \theta > \theta_{fu} + \delta/2 \end{cases} \tag{21}$$

wherein the above equation, $\theta_{fu}$ is the dimensionless fusion temperature:

$$\theta_{fu} = \frac{T_{fu} - T_c}{\Delta T} \tag{22}$$

Invoking the dimensionless variables of Eq. (12), the boundaries Eq. (4) are transformed into:

$$\forall\ X,\ Y | (X - X_i)^2 + (Y - Y_i)^2 = R_i^2 \ \Rightarrow U = V = 0,\ \theta = 1$$
$$\forall\ X,\ Y | X^2 + Y^2 = R_o^2 \ \Rightarrow U = V = 0,\ \theta = 0$$
$$\forall\ X,\ Y | (X - R_o\cos(\omega))^2 + (Y - R_o\sin(\omega))^2 = R_i^2 \ \Rightarrow U = V = 0,\ \theta = 1$$
$$\forall\ X,\ Y | (X - R_o\cos(\omega))^2 + (Y - R_o\sin(\omega))^2 = R_o^2 \ \Rightarrow U = V = 0,\ \theta = 0$$
$$\forall\ X,\ Y \left| \begin{array}{l} 0 \le X \le (R_o - R_i)\cos(\omega),\ 0 \le y \le (R_o - R_i)\sin(\omega) \\ \Rightarrow U = V = 0,\ \frac{\partial\theta}{\partial n} = 0 \\ (R_o + R_i)\cos(\omega) \le X \le 2R_o\cos(\omega), \\ (R_o + R_i)\cos(\omega) \le Y \le 2R_o\sin(\omega) \end{array} \right| \Rightarrow U = V = 0$$
$$, \frac{\partial\theta}{\partial n} = 0 \tag{23}$$

The local Nusselt at the hot wall can be introduced employing the energy balance as:

$$Nu_l = -(1 + Nc\phi)\left(\frac{\partial\theta}{\partial n}\right)_{(X-R_i\cos(\omega))^2+(Y-R_i\sin(\omega))^2=R_i^2} \quad (24)$$

Then, $Nu_l$ is integrated over the hot wall to produce the average Nusselt number:

$$Nu_a = \frac{1}{\pi}\int_0^{\pi} Nu_l d\omega \quad (25)$$

Here, the presence of nanoparticles will change the average Nusselt number. Hence, $Nu_r$ is introduced to judge the heat transfer improvement of NEPCM suspension compared to water.

$$Nu_r = \frac{Nu_a|_{\phi}}{Nu_a|_{\phi=0}} \quad (26a)$$

The presence of the nanoparticles in the base fluid changes the thermophysical properties such as sensible heat, thermal conductivity, dynamic viscosity, and the density of the host fluid. The nanoparticles would also contribute to heat transfer by their latent heat of fusion. The case of $Ste\to\infty$, represents a NEPCM-suspension with no phase change. Thus, the impact of nanoparticles with no phase change was examined on heat transfer by introducing $Nu_r'$. This parameter shows the heat transfer enhancement of NEPCM-suspension with no phase change compared to the base fluid:

$$Nu_r^{'} = \frac{Nu_a|_{\phi,Ste\to\infty}}{Nu_a|_{\phi=0}} \quad (26b)$$

Finally, $Nu_r''$ compares the impact of phase change of nanoparticles to the same nanofluid but without phase change. Here $Nu_r''$ is defined as.

$$Nu_r^{''} = \frac{Nu_r^{'}}{Nu_r} = \frac{Nu_a|_{\phi}}{Nu_a|_{\phi,Ste\to\infty}} \quad (26c)$$

Indeed, $Nu_r''$ is an indication of the benefit of the latent heat of nanoparticles on heat transfer.

In addition, the entropy generation relation was transformed into a dimensionless form as:

$$S_{TO} = S_T + S_V = \frac{k_b}{k_f}\left[\left(\frac{\partial\theta}{\partial X}\right)^2 + \left(\frac{\partial\theta}{\partial Y}\right)^2\right] + \chi\frac{\mu_b}{\mu_f}\left(2\left(\frac{\partial U}{\partial X}\right)^2 + 2\left(\frac{\partial V}{\partial Y}\right)^2 + \left(\frac{\partial U}{\partial Y} + \frac{\partial V}{\partial X}\right)^2\right) \quad (27)$$

In the above equation, $\chi$ indicates the irreversibility parameter:

$$\chi = \frac{\mu_f T_0}{k_f}\left(\frac{\alpha_f}{H(T_h - T_c)}\right)^2 \quad (28)$$

The Bejan number is introduced as a factor of the magnitude of friction irreversibility to the total entropy generation by:

$$Be = \frac{\int_A S_T dA}{\int_A S_{TO} dA} \quad (29)$$

## 3. Numerical approach

### 3.1. Grid test

Galerkin finite element method was applied to solve the equations numerically. However, the equations had been transformed into the weak form before the solution. Grid study and independency play a vital role in all numerical studies. A structured type of grids was provided for the annular domain, which is shown in Fig. 2. In this regard, five different meshes with different element sizes were examined for the domain study: Case I; 50 × 100, Case II; 100 × 150, Case III; 150 × 200, Case IV; 200 × 250, Case V; 250 × 3000, and Case VI; 300 × 350. Table 2 indicates the average Nusselt number and max streamline value for these five case when $Ra = 10^6$, $Ste = 0.2$, $\phi = 0.04$, $\theta_f = 0.5$, and $\omega = 45^\circ$. It is evident that the difference between the results of Cases III, IV, V, and VI is insignificant. In addition, according to Fig. 3, the phase transition zone ($Cr$) of the suspension for all the cases is similar. So, due to reduce the time of simulations, the third case was chosen for all simulations.

### 3.2. Validation

The present research was validated with achievable experimental and numerical investigations. In this regard, Habibi Matin and Pop [33] validate the results of the present work with the literature numerical investigations. They were carried out their studies on an eccentric ring filled with Cu-water nanofluid.

They studied the effects of eccentricity ($\varepsilon$), the ratio of external radius to the internal radius ($R_r$), the nanoparticle concentration ($\phi$), and the $Ra$ on the average Nusselt number, isotherms, and streamlines. Fig. 4 indicates the values of average Nusselt number of Ref. [47] (I) and this study (II) for different nanoparticle volume fractions when eccentricity $\varepsilon = 0.5$, radius ratio $Pr = 6.21$, $Ra = 10^6$, and $R_r = 2.5$. A good agreement is seen between the results of two studies.

The results were also verified by the experimental and numerical investigations of Cesini and et al. [48]. They examined the free convection heat transfer of a horizontal circular-cylinder placed inside a cavity in which the air was the working fluid. The vertical walls of the cavity were isotherm ($T_c$), and the cylinder surface was in constant hot temperature ($T_h$), and the bottom wall of the cavity was adiabatic. Fig. 5 shows the comparison between the results of current work and numerical and experimental results of Ref. [48], in which the values of the average Nusselt number for three different Rayleigh numbers were reported. According to Fig. 5, a reasonable agreement between the results of there two researches is evident.

Finally, the results of the present work were validated with numerical research of Ilis et al. [49]. These researches investigated the heat transfer, fluid friction, and entropy generation of a cavity with different aspect ration ($AR$). The horizontal walls were adiabatic, and the vertical walls of the cavity were considered at constant temperatures $T_h$ (left wall) and $T_c$ (right wall), respectively. Fig. 6(a) and (b) depict the local entropy generation due to heat transfer and fluid friction for the current study (dots) and Ref. [49] (graph) when $AR = 1$, $\chi = 10^{-4}$, and $Ra = 10^5$. A desirable agreement between the results of these researches could be approved.

## 4. Results and discussions

In the current research, the thermal and hydrodynamic behavior of a NEPCM-suspension is addressed in annuli of the eccentric horizontal cylinders. According to the data reported in Barlak et al. [40], the ratio of the thermal conductivity of the suspension to the base fluid for the

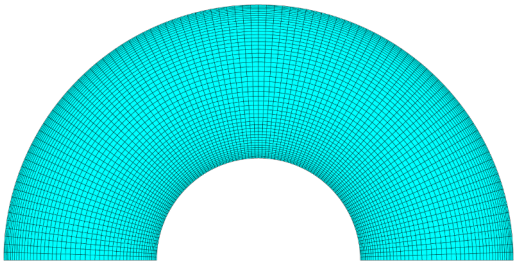

**Fig. 2.** The structured mesh of size 50 × 100.

**Table 2**
Grid independence test for $Ra = 10^6$, $Ste = 0.2$, $\phi = 0.04$, $\theta_f = 0.5$, and $\omega = 45^\circ$.

| Case number | One | Two | Three | Four | Five | Six |
|---|---|---|---|---|---|---|
| No. of elements | (50 × 100) | (100 × 150) | (150 × 200) | (200 × 250) | (250 × 300) | (300 × 350) |
| $\Psi_{max}$ | 30.2121 | 30.2621 | 30.2738 | 30.2487 | 30.2463 | 30.2455 |
| $Nu_a$ | 11.5247 | 11.5388 | 11.5453 | 11.5478 | 11.5486 | 11.5489 |

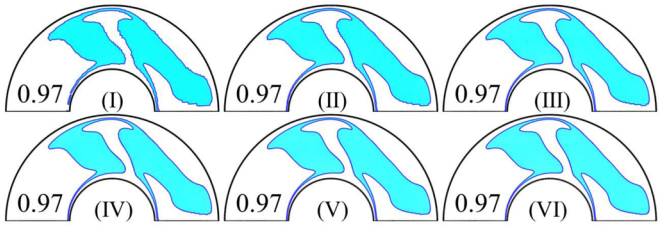


**Fig. 3.** The *Cr* contours for different gird sizes.

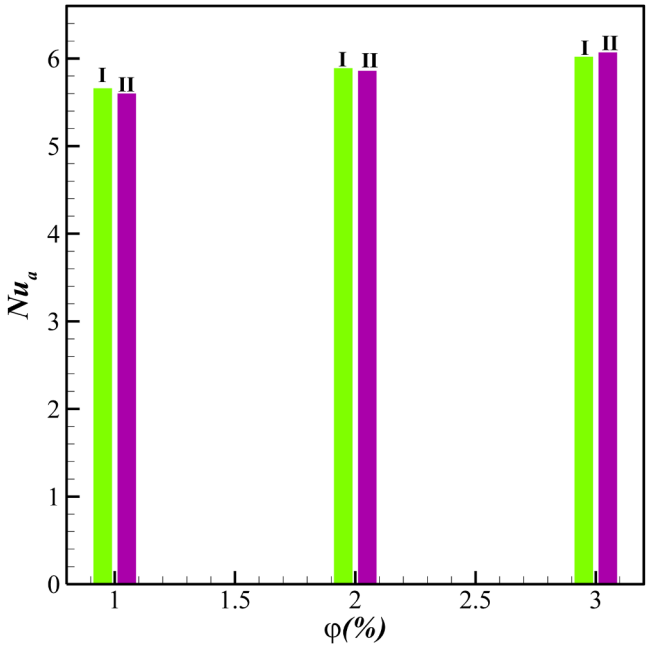


**Fig. 4.** Average Nusselt number of Ref. [47] (I) and present work (II) when $Pr = 6.21$, eccentricity $\varepsilon = 0.5$, radius ratio $R_r = 2.5$, and $Ra = 10^6$.

$\phi = 0.04$ is 1.24. Also, this ratio for the dynamic viscosity is 1.5. Also, the sensible heat capacity ratio λ reported by Barlak et al. [40] is 0.32. The radii ratio, i.e., $R_r$, is fixed at 2.5. The simulations are carried out for the control parameters in the following range: $10^4 \le Ra \le 10^6$, $0.2 \le Ste \le 100$, $0.05 \le \theta_f \le 1$, $0 \le \omega \le \pi/2$, and two volume-concentrations of $\phi = 0.0$ and 4%. The typical value of the non-dimensional parameters was selected as $Pr = 6.2$, $Ra = 10^5$, $\theta_f = 0.5$, $Ste = 0.2$, $\phi = 0.04$, $R_r = 2.5$, $Nc = 6.0$, $\lambda = 0.322$, $Nv = 12.5$, $\omega = 0^\circ$. These values will be adopted as reference and will be not repeated in the text. The value of a parameter will be reported only if its value is different of the reference value.

The streamlines, the isotherms, and the contours of the heat capacity ratio *Cr* are represented in Fig. 7 for various values of Rayleigh number, i.e., *Ra*. The flow patterns are similar in all cases and present a symmetry around the cavity center. The fluid surrounding the inner hot cylinder heats up and moves upward while the colder one near the outer cylinder moving downwards and convective flow takes place. Two recirculation zones with opposite rotation directions are thus created in the cavity. For $Ra = 10^4$, the streamlines are concentric elliptic curves. As *Ra* is raised, the intensity of the flow is increased, and

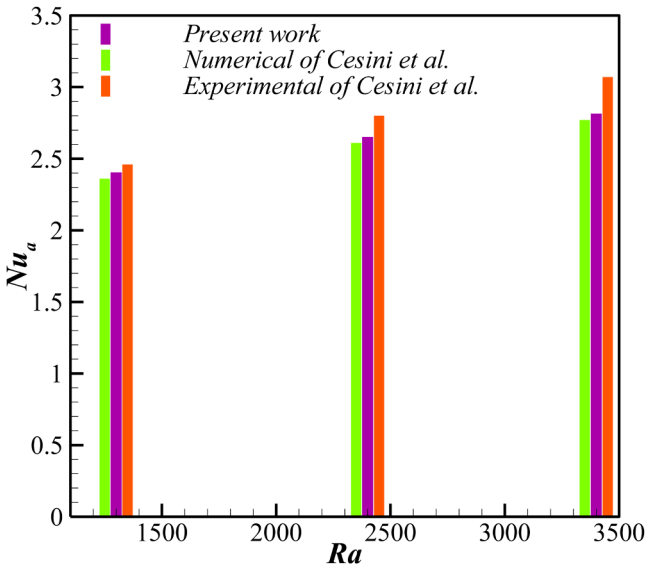


**Fig. 5.** the average Nusselt number of the present work and Ref. [48] in three different Rayleigh numbers.

an additional vortex appears inside the recirculation zones near the channel center. The isothermal contours are affected by the flow development in the cavity. While the isotherms of high temperature remain concentrated near the hot wall, the isotherms of lower temperature are longer when *Ra* is increased, indicating that the zone occupied by the fluid at a given temperature grows in size for higher *Ra* due to the enhanced mixing associated to higher convection effects.

The *Cr* contours show the area where the nanoparticles are at the fusion temperature and experience the phase change. This zone is colored in blue in the graph. It is evident that the phase change zone increases in size for higher *Ra*. Indeed, a phase change occurs when the liquid temperature is about the particles' fusion temperature, i.e., $\theta_f$. As the isotherm corresponding to $\theta_f$ is longer when *Ra* is increased, the zone of the fluid having this temperature grows, and consequently, the zone where the NEPCM undergo phase change is large.

Fig. 8 depicts the effect of the tilting angle of the cavity, i.e., $\omega$, on the streamlines, the isotherms, and the contours of *Cr*. For $\omega = 0^\circ$, as discussed in Fig. 7 and shown in Fig. 8, the flow patterns present a symmetry around the cavity center. As $\omega$ is increased to 45°, this symmetry vanishes, and the recirculation zone in the anti-clockwise direction gets larger due to the increased available space for its circulation.

For $\omega = 90^\circ$, which corresponds to the case where the cavity is vertical, and the heated inner cylinder is at the right, the two recirculation zones merge into one large eddy covering most of the cavity and concentrate at the top where the convective effects are strong. The symmetry if the isothermal contours for $\omega = 0^\circ$ is slightly disturbed when $\omega$ reaches 45°, but an important difference appears for $\omega = 90^\circ$ where the isotherms are distorted and concentrated mainly at the top cavity due to increased convective effects in that region. The phase change zone follows the temperature distribution in the cavity. A small change in this zone appears between $\omega = 0^\circ$ and $\omega = 45^\circ$ while most of the phase change of the core of the NEPCM particles occurs at the top of

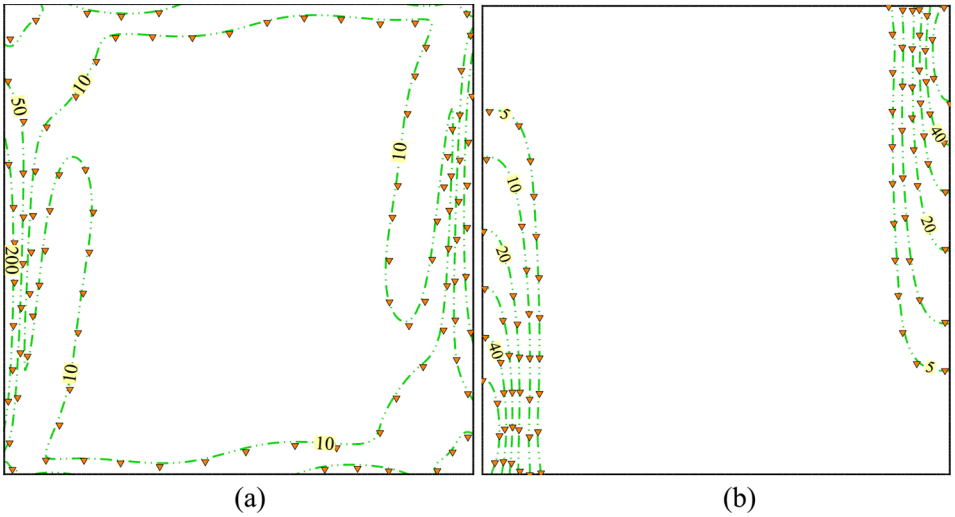


**Fig. 6.** the comparison of a) heat transfer entropy generation and b) fluid friction entropy generation between current study (dots) and Ref. [49] when $AR = 1$, $\chi = 10^{-4}$ and $Ra = 10^5$.

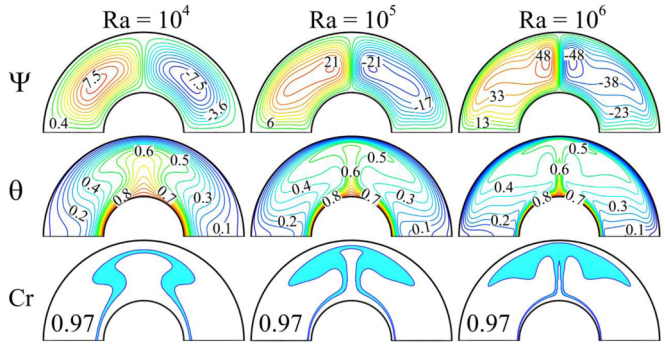


**Fig. 7.** Influence of the Rayleigh number on the streamlines, isotherms and the phase transition zone (*Cr*) of the suspension.

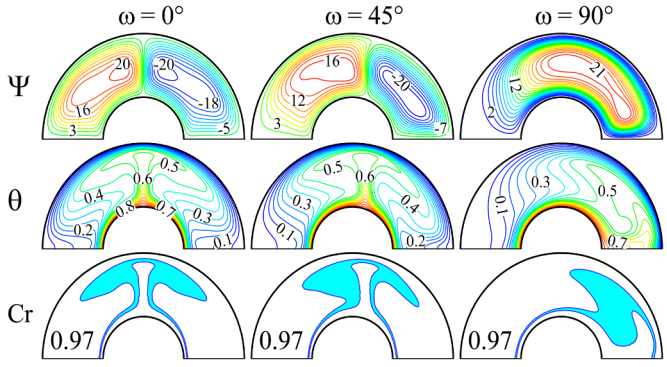


**Fig. 8.** Effect of inclination angle on the streamlines, isotherms and the phase transition zone (*Cr*).

the cavity when it is oriented vertically for $\omega = 90^\circ$.

Fig. 9 shows the isentropic lines corresponding to the entropy generation by heat transfer $S_T$, by the liquid friction $S_V$, and the total entropy $S_{TO}$ for different values of *Ra*. For low *Ra*, the isentropic lines by heat transfer are mainly concentrated near the walls, due to the high temperature-gradients in that region. In fact, as the buoyancy forces are diminished for low *Ra*, heat transfer is dominated by conduction and focused in that region. As *Ra* is increased, convective heat transfer intensifies, and the entropy generation by heat transfer $S_T$ increases. The entropy generation is also concentrated near the cavity walls due to the increased viscous friction between the layers of the fluid in that region. When *Ra* is increased, the flow intensifies, and a growth in entropy generation $S_V$ can be observed in the cavity center, at the border between the two recirculation zones covering the channel. As both types of entropy generation with *Ra*, the total entropy generation $S_{TO}$ is higher when *Ra* is raised.

The isentropic lines corresponding to the entropy generation in the cavity for various values of $\omega$ are plotted in Fig. 10 For $\omega = 0^\circ$, the isentropic lines are symmetrically distributed around the channel center. As $\omega$ is increased, the cavity is tilted and the concentration of the isentropic lines shifts toward the right part of the cavity, and when the cavity is vertical ($\omega = 90^\circ$), the entropy generation is focused in the upper part of the enclosure where the convective flow is mainly intensified. Related to the intensity of convective heat transfer, the corresponding entropy generation decreases for higher $\omega$. Nonetheless, as the entropy generation related to the flow-friction is increased for higher $\omega$, which leads to an increase in the total heat transfer.

The variation of the average Nusselt number $Nu_a$ as a function of the fusion temperature $\theta_f$ is shown in Fig. 11 for different values of Stefan number, i.e., *Ste*. First, it can be seen that $Nu_a$ is minimum for $\theta_f = 1$ then for $\theta_f = 0$, as in these cases, the phase change of the NEPCM is limited to the region surrounding the inner cylinder and the outer cylinder respectively, so only a few numbers of particles experience phase change. $Nu_a$ increases when the fusion temperature is not close to the wall temperatures. The Nusselt number is maximum for $\theta_f = 0.2$ and $\theta_f = 0.6$, while it reaches a local minimum value for $\theta_f = 0.4$.

In addition, $Nu_a$ can increase by 8% when *Ste* is reduced from 100 to

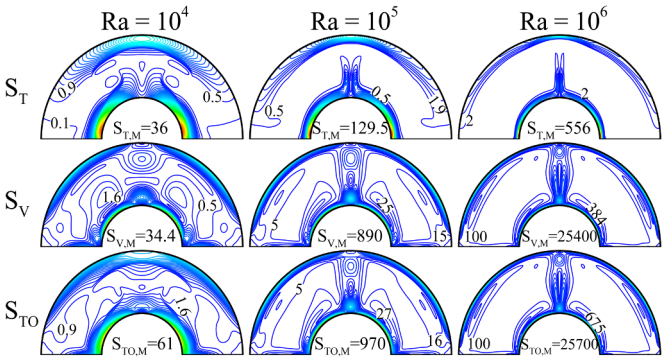


**Fig. 9.** Effect of the Rayleigh number on the isentropic lines ($S_T$, $S_V$ and $S_{TO}$) at $Pr = 6.2$, $\theta_f = 0.5$, $Ste = 0.2$, $\phi = 0.04$, $R_r = 2.5$, $\omega = 0^\circ$, $Rr = 2.5$, $Nc = 6.0$, $\lambda = 0.322$, and $Nv = 12.5$.

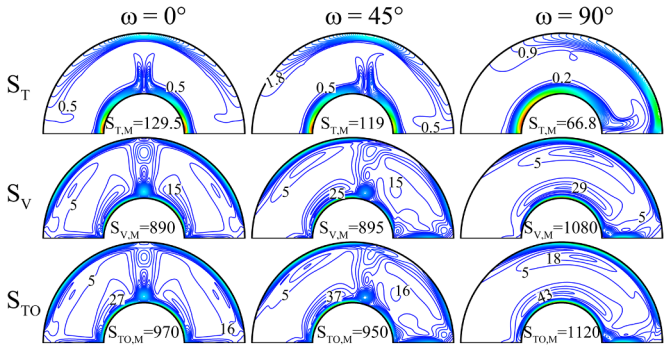


**Fig. 10.** Effect of inclination angle on the isentropic lines ($S_T$, $S_V$ and $S_{TO}$).

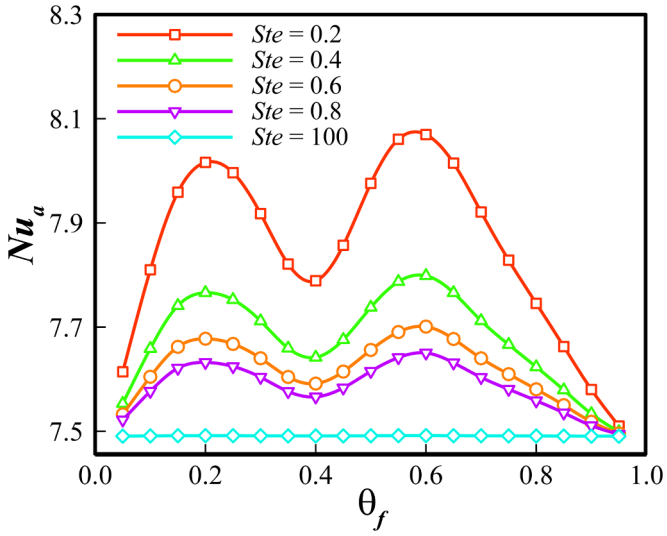


**Fig. 11.** Variation of the average Nusselt number with the non-dimensional fusion temperature and the Stefan number of the NEPCMs.

0.2. In fact, a higher value of *Ste* is associated with a lower latent heat of the NEPCM core. So when *Ste* is raised, the latent heat of the NEPCM particles decreases and the involvement of these nanoparticles in the overall heat transfer diminishes, which leads to a lower value of $Nu_a$.

The impact of $\omega$ on the $Nu_a$ as a function of $\theta_f$ is illustrated in Fig. 12. It can be seen that $Nu_a$ increases when $\omega$ is reduced. It is maximum when the cavity is horizontal ($\omega = 0^\circ$) and minimum when the cavity is vertical ($\omega = 90^\circ$). A 30% increase in the value of $Nu_a$ can be reached by changing the orientation of the cavity. For $\omega = 0^\circ$, the inner hot cylinder is located at the bottom while the outer cold one is at the top, optimizing the free convection in the enclosure. When $\omega$ is increased, the hot cylinder shifts toward the right and the free convection is relatively inhibited; thus, $Nu_a$ was reduced. In addition, the maximum and minimum values of $Nu_a$ for different values of $\omega$ can be found at different values of $\theta_f$. This is attributed to the number of particles experiencing the phase change, which varies with $\theta_f$.

Fig. 13 depicts the variation of Bejan number, i.e., *Be*, as a function of $\theta_f$ for various values of $\omega$. First, it can be seen that, in all cases, $Be < 0.2$. This indicates that the entropy generation in the cavity is dominated by fluid friction. Nonetheless, it is shown that for all the values of $\omega$, the value of *Be* is maximum when $\theta_f$ is around 0.4, while it is minimum for $\theta_f = 1$.

Moreover, *Be* is at its lowest value when the cavity is horizontal ($\omega = 0^\circ$) for low $\theta_f$ ($\theta_f < 0.3$) and when it is vertical ($\omega = 90^\circ$) for high $\theta_f$ ($\theta_f > 0.7$). When $\theta_f < 0.1$, In that case, *Be* is maximized in a vertical cavity. In fact, the frictional entropy generation is very intense in a vertical-cavity near the upper wall and in a horizontal cavity near the walls and around the center, dominating the heat transfer entropy and leading to a relatively lower value of *Be* compared to the other configurations.

The Bejan number as a function of $\theta_f$ is visualized in Fig. 14 for selected values of *Ste*. *Be* decreases with the rise of *Ste* for all the values of $\theta_f$. This underlines the contribution of the phase-change latent heat of the NEPCM core to the production of entropy by heat transfer. This can also be seen by the fact that when *Ste* is very high, *Be* remains constant.

Fig. 15 illustrates $Nu_a$ as a function of $\omega$ for various *Ra* and nanoparticle concentrations. For all the values of $\omega$, it can be seen that $Nu_a$ substantially increases when *Ra* is raised. Nonetheless, when $Ra = 10^4$ and $Ra = 10^5$, the effect of $\omega$ on the reduction of $Nu_a$ is not high compared to $Ra = 10^6$. This is due to the effects of the buoyancy forces, which are more developed at $Ra = 10^6$. So, the severity of the effect of $\omega$ on the $Nu_a$ is different for low and high *Ra*.

Moreover, it is shown that for the various values of *Ra*, $Nu_a$ is higher when a volume fraction $\phi = 0.04$ of the NEPCM particles is used compared to a fluid without NEPCM particles ($\phi = 0$), pointing out the contribution of the nanoparticles to the heat transfer in the enclosure. Notably, a 350% rise in the value of $Nu_a$ can be found when *Ra* and $\phi$ are increased from $10^4$ and 0 to $10^6$ and 0.04, respectively.

Fig. 16 shows the Bejan number as a function of $\omega$ for different values of *Ra* and $\phi$. First, it is shown that *Be* increase when the value of *Ra* is raised. Indeed, when *Ra* is increased, a stronger flow takes place, and convective heat transfer is enhanced. This simultaneously tends to raise the entropy generation by heat transfer and reduce the one by fluid friction.

In addition, it can be seen that using a higher value of $\phi$ slightly reduces *Be* for low *Ra*, but leads to the opposite for high *Ra*. In fact, for low *Ra*, the flow is dominated by viscous forces, and convective heat transfer is relatively inhibited. The effect of the NEPCM particles is limited to the increase of the viscosity of the fluid and contributes to the increase of the entropy generation by viscous friction, thus decreasing the value of *Be*. On the other hand, when *Ra* is increased, the viscous effects are negligible, and the effect of the NEPCM particles lays in their involvement in the heat transfer, which intensifies the entropy generation by heat transfer compared to fluid friction, and, consequently, *Be* increases.

Table 3 summarizes the impact of the different parameters on the different defined Nusselt numbers $Nu_a$, $Nu_r'$ and $Nu_r''$. As discussed earlier, $Nu_a$ rises when *Ra* increases, and when *Ste* and $\omega$ are reduced. $Nu_r'$, which represents the effect of the presence of NEPCM particles without phase change compared to a pure fluid, also increases with *Ra* due to the increase of convective effects irrespective of the presence of

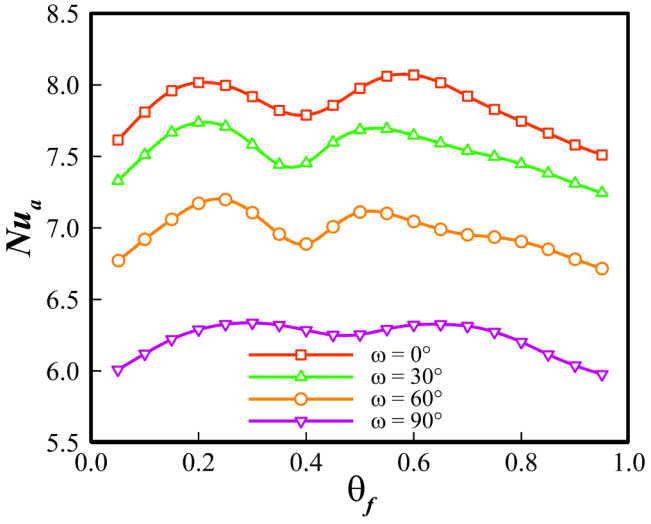


**Fig. 12.** Variation of the average Nusselt number with the non-dimensional fusion temperature and the inclination angle of the NEPCMs.

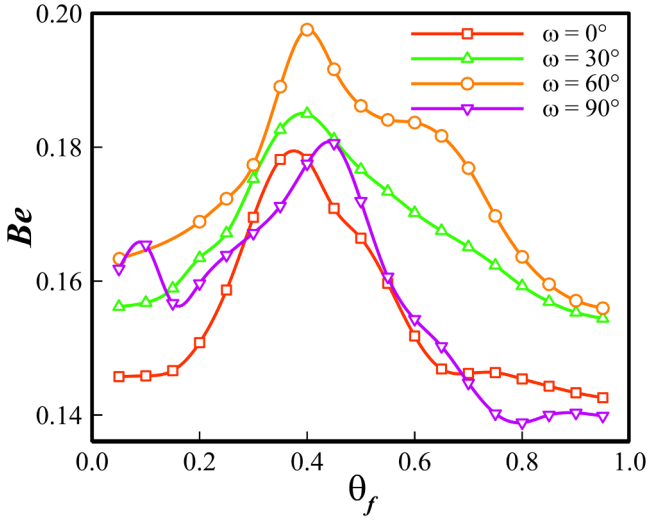


**Fig. 13.** Variation of the average Bejan number with the non-dimensional fusion temperature and the inclination angle of the NEPCMs.

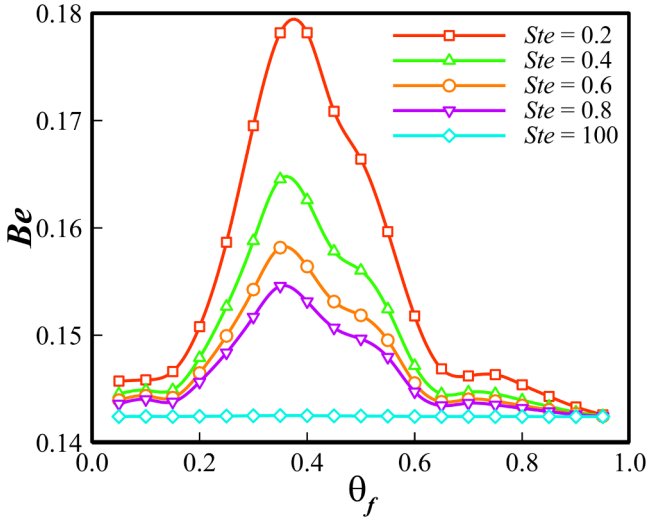


**Fig. 14.** Variation of the average Bejan number with the non-dimensional fusion temperature and the Stefan number of the NEPCMs.

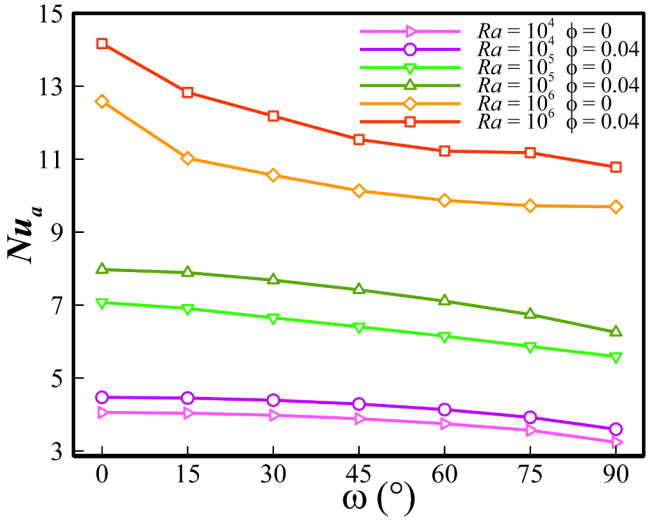


**Fig. 15.** Variation of the average Nusselt number with inclination angle and the Rayleigh number of the NEPCMs for various $\phi$.

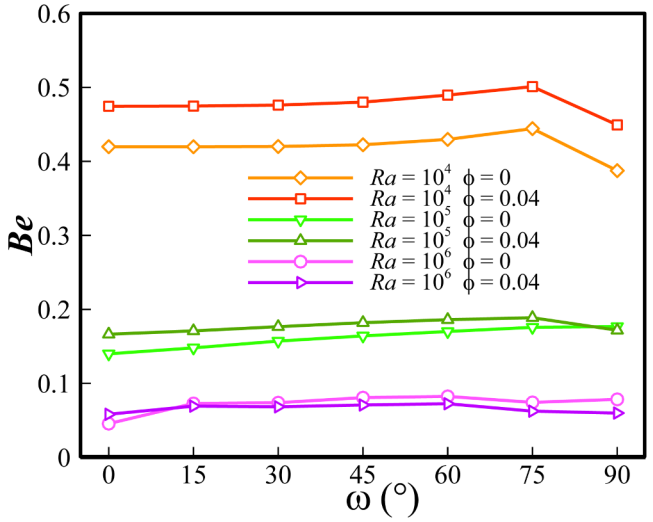


**Fig. 16.** Variation of the average Bejan number with inclination angle and the Rayleigh number of the NEPCMs for various $\phi$.

**Table 3**
Impact of control parameters on the average Nusselt numbers, and Nusselt number ratios ($Pr$ = 6.2, $R_r$ = 2.5, $Nc$ = 6.0, $\lambda$ = 0.322, and $Nv$ = 12.5).

| $Ra$ | $\omega$ | $Ste$ | $\theta_f$ | $\phi$ | $Nu_a$ | $Nu_r'$ | $Nu_r''$ |
|---|---|---|---|---|---|---|---|
| $10^6$ | 0 | 0.2 | 0.5 | 0.00 | 12.5945 | 1 | 1 |
| $10^6$ | 0 | 0.2 | 0.5 | 0.04 | 14.1679 | 1.0515 | 1.0697 |
| $10^6$ | 0 | 0.2 | 0.1 | 0.04 | 13.8220 | 1.0514 | 1.0437 |
| $10^6$ | 0 | 100 | 0.5 | 0.04 | 13.2436 | 1.0515 | 1 |
| $10^6$ | 45 | 0.2 | 0.5 | 0.04 | 11.5453 | 1.0777 | 1.0563 |
| $10^5$ | 0 | 0.2 | 0.5 | 0.04 | 7.9759 | 1.0589 | 1.0646 |
| $10^4$ | 0 | 0.2 | 0.5 | 0.04 | 4.4712 | 1.0293 | 1.0708 |

the NEPCM particles. It is clear that $Nu_r'$ is greater than 1 for all the cases where $\phi$ = 0.04 indicating an increase of the heat transfer due to the presence of the particles. $Nu_r'$ does not change when $Ste$ and $\theta_f$ are varied as no phase change takes place. $Nu_r'$ increases when $\omega$ is increased from 0 to 45°, meaning that the effect of the presence of the NEPCM particles is more apparent when the cavity is tilted. On the other hand, $Nu_r''$ underlines the influence of the phase change of the NEPCM particles on the value of $Nu_a$. It can be seen that there is no impact of the phase change ($Nu_r''$ = 1) when $\phi$ = 0 or when $Ste$ = 100, i.e., when there are no NEPCM particles in the flow or when the latent heat of the NEPCM core is negligible. It is shown that the fusion temperature is one of the key parameters, which controls the heat transfer behavior of the suspension.

## 5. Conclusion

In the current research, the convective heat transfer and entropy generation of a NEPCM- suspension were examined in an enclosure. A CFD model for the natural convection flow, heat transfer, and entropy generation of the suspension, including the phase change terms, was introduced. Then, the FEM was applied to solve the governing equations in a Cartesian coordinate system numerically. The validations and verifications with literature works were performed, and the results were found in good agreement. The main results of the present study can be summarized as:

Using a higher value of the volume fraction of the NEPCM particles leads to a better rate of heat transfer, as more particles are undergoing phase change at their core and contributing to heat transfer.

The fusion temperature, $\theta_f$, of the NEPCM affects heat transfer, which is inhibited when $\theta_f$ is near to the temperature of the hot or cold cylinder, as phase change would be limited to the near-wall regions in

that case. Conversely, and due to the temperature distribution in the enclosure, the best heat transfer is achieved when $\theta_f$ is around 0.2 or 0.6.

Increasing *Ste*, indicating a lower latent heat of the NEPCM core, inhibits heat transfer. This emphasizes the contribution of the phase change latent heat of the NEPCM to the total heat transfer in the cavity.

Heat transfer is affected by the inclination angle of the cavity $\omega$. While it is maximum in a horizontal cavity where the inner heated cylinder is at the bottom, it starts to diminish when $\omega$ is increased and reaches its minimum in a vertical-cavity where the convective flow is concentrated in the upper part. The effect of $\omega$ on heat transfer is severe at high *Ra*.

The entropy generation owing to fluid friction is higher compared to the entropy generation by heat transfer in all the considered cases.

However, the relative importance of the latter grows when *Ra* is raised and when *Ste* is decreased, indicating the involvement of the NEPCM core undergoing phase change in the entropy generation by heat transfer in the cavity.

Using a higher volume fraction of the NEPCM particles inhibits the entropy generation by heat transfer for low *Ra* where viscous effects are dominating the flow, but enhances it for high *Ra* when viscous forces are negligible with respect to the buoyancy forces driving the flow. Furthermore, the gross entropy generation increases with *Ra* and $\omega$.

## CRediT authorship contribution statement

**Mehdi Ghalambaz:** Conceptualization, Methodology, Software, Validation, Formal analysis, Data curation. **S.A.M. Mehryan:** Visualization, Writing - original draft, Investigation, Formal analysis, Data curation. **Masoud Mozaffari:** Methodology, Software, Formal analysis, Data curation. **Ahmad Hajjar:** Investigation, Formal analysis, Writing - review & editing. **Mohamad El Kadri:** Conceptualization, Investigation, Supervision, Writing - review & editing. **Nesrine Rachedi:** Software, Data curation, Writing - review & editing. **Mikhail Sheremet:** Investigation, Writing - review & editing. **Obai Younis:** Conceptualization, Writing - review & editing, Investigation. **Sohail Nadeem:** Writing - review & editing, Supervision.

## Declaration of Competing Interest

None

## Acknowledgments

This work of Mikhail A. Sheremet was conducted as a government task of the Ministry of Science and Higher Education of the Russian Federation (Project Number 0721–2020–0036).

## References

[1] R. Chen, et al., Electro/photo to heat conversion system based on polyurethane embedded graphite foam, Appl. Energy 152 (2015) 183–188.
[2] K. Venkatadri, et al., Melting heat transfer analysis on magnetohydrodynamics buoyancy convection in an enclosure: a numerical study, J. Appl. Comput. Mech. 6 (1) (2020) 52–62.
[3] W. Hu, et al., A modeling study on the heat storage and release characteristics of a phase change material based double-spiral coiled heat exchanger in an air source heat pump for defrosting, Appl. Energy 236 (2019) 877–892.
[4] M. Emam, S. Ookawara, M. Ahmed, *Thermal management of electronic devices and concentrator photovoltaic systems using phase change material heat sinks: experimental investigations*, Renew. Energy 141 (2019) 322–339.
[5] N. Aslfattahi, et al., Experimental investigation of energy storage properties and thermal conductivity of a novel organic phase change material/MXene as A new class of nanocomposites, J. Energy Storage 27 (2020) 101115.
[6] T.H. Kean, et al., Numerical study on heat transfer performance enhancement of phase change material by nanoparticles: a review, J. Adv. Res. Fluid Mech. Therm. Sci. 45 (1) (2018) 55–63.
[7] Y. Krishna, et al., Enhancing the thermal properties of organic phase change material (palmitic acid) by doping MXene nanoflakes, AIP Conference Proceedings, AIP Publishing LLC, 2020.
[8] Y. Krishna, et al., Fatty acid/metal ion composite as thermal energy storage materials, SN Applied Sci. 2 (5) (2020) 1–10.
[9] M.A. Sheremet, N. Bondareva, F.-.Y. Zhao, The brick thermal performance improvement using phase change materials, J. Appl. Comput. Mech. (2020).
[10] Y. Zhu, et al., *Nanoencapsulated phase change materials with polymer-SiO2 hybrid shell materials: compositions, morphologies, and properties*, Energy Convers. Manage. 164 (2018) 83–92.
[11] A. Soottitantawat, et al., *Microencapsulation by Spray Drying: influence of Emulsion Size on the Retention of Volatile Compounds*, J. Food Sci. 68 (7) (2003) 2256–2262.
[12] F. Caruso, et al., Enzyme Encapsulation in Layer-by-Layer Engineered Polymer Multilayer Capsules, Langmuir 16 (4) (2000) 1485–1488.
[13] D.G. Shchukin, et al., Layer-by-Layer Assembled Nanocontainers for Self-Healing Corrosion Protection, Adv. Mater. 18 (13) (2006) 1672–1678.
[14] J.-.F. Su, L.-.X. Wang, L. Ren, *Synthesis of polyurethane microPCMs containing n-octadecane by interfacial polycondensation: influence of styrene-maleic anhydride as a surfactant*, Colloids and Surfaces A: Physicochemical and Engineering Aspects 299 (1–3) (2007) 268–275.
[15] G. Fang, et al., Preparation and characterization of nano-encapsulated n-tetradecane as phase change material for thermal energy storage, Chem. Eng. J. 153 (1–3) (2009) 217–221.
[16] J.M. Asua, Challenges for industrialization of miniemulsion polymerization, Prog. Polym. Sci. 39 (10) (2014) 1797–1826.
[17] E.M. Shchukina, et al., Nanoencapsulation of phase change materials for advanced thermal energy storage systems, Chem. Soc. Rev. 47 (11) (2018) 4156–4175.
[18] Y. Zhu, et al., Morphological control and thermal properties of nanoencapsulated n-octadecane phase change material with organosilica shell materials, Energy Convers. Manage. 119 (2016) 151–162.
[19] R. Ciriminna, et al., *From Molecules to Systems: sol−Gel Microencapsulation in Silica-Based Materials*, Chem. Rev. 111 (2) (2011) 765–789.
[20] W. Fu, et al., Thermophysical properties of n -tetradecane@polystyrene-silica composite nanoencapsulated phase change material slurry for cold energy storage, Energy Build 136 (2017) 26–32.
[21] S. Ushak, et al., Preparation and Characterization of Inorganic PCM Microcapsules by Fluidized Bed Method, Materials (Basel) 9 (1) (2016).
[22] A.M. Rashad, et al., *Entropy generation and MHD natural convection of a nanofluid in an inclined square porous cavity: effects of a heat sink and source size and location*, Chin J. Phys. 56 (1) (2018) 193–211.
[23] M. Sheikholeslami, et al., Variable magnetic forces impact on magnetizable hybrid nanofluid heat transfer through a circular cavity, J. Mol. Liq. 277 (2019) 388–396.
[24] N.A.C. Sidik, et al., Recent progress on hybrid nanofluids in heat transfer applications: a comprehensive review, Int. Commun. Heat Mass Transf. 78 (2016) 68–79.
[25] Y. Krishna, et al., State-of-the-art heat transfer fluids for parabolic trough collector, Int. J. Heat Mass Transf. 152 (2020) 119541.
[26] A.I. Alsabery, et al., Two-phase nanofluid model and magnetic field effects on mixed convection in a lid-driven cavity containing heated triangular wall, Alexandria Eng. J. 59 (1) (2020) 129–148.
[27] A.I. Alsabery, et al., Effect of nonhomogeneous nanofluid model on transient natural convection in a non-Darcy porous cavity containing an inner solid body, Int. Commun. Heat Mass Transf. 110 (2020).
[28] G.R. Kefayati, et al., Lattice Boltzmann simulation of natural convection in tall enclosures using water/SiO2 nanofluid, Int. Commun. Heat Mass Transf. 38 (6) (2011) 798–805.
[29] G. Kefayati, et al., Lattice Boltzmann simulation of natural convection in an open enclosure subjugated to water/copper nanofluid, Int. J. Therm. Sci. 52 (2012) 91–101.
[30] D. Yadav, The density-driven nanofluid convection in an anisotropic porous medium layer with rotation and variable gravity field: a numerical investigation, J. Appl. Comput. Mech. 6 (3) (2020) 699–712.
[31] N. Aslfattahi, et al., Experimental investigation on thermal stability and enthalpy of eutectic alkali metal solar salt dispersed with MgO nanoparticles, The 4th International tropical renewable energy conference, 2019.
[32] G.R. Kefayati, FDLBM simulation of entropy generation due to natural convection in an enclosure filled with non-Newtonian nanofluid, Powder Technol. 273 (2015) 176–190.
[33] C.J. Ho, et al., Water-based suspensions of Al2O3 nanoparticles and MEPCM particles on convection effectiveness in a circular tube, Int. J. Therm. Sci. 50 (5) (2011) 736–748.
[34] H. Reza Seyf, et al., Flow and Heat Transfer of Nanoencapsulated Phase Change Material Slurry Past a Unconfined Square Cylinder, J. Heat Transf. 136 (5) (2014).
[35] M. Ghalambaz, A.J. Chamkha, D. Wen, Natural convective flow and heat transfer of Nano-Encapsulated Phase Change Materials (NEPCMs) in a cavity, Int. J. Heat Mass Transf. 138 (2019) 738–749.
[36] M. Ghalambaz, et al., Unsteady natural convection flow of a suspension comprising Nano-Encapsulated Phase Change Materials (NEPCMs) in a porous medium, Advanced Powder Technol. 31 (3) (2020) 954–966.
[37] A. Hajjar, S.A.M. Mehryan, M. Ghalambaz, Time periodic natural convection heat transfer in a nano-encapsulated phase-change suspension, Int. J. Mech. Sci. 166 (2020).
[38] S. Mehryan, et al., Natural convection flow of a suspension containing nano-encapsulated phase change particles in an eccentric annulus, J. Energy Storage 28 (2020) 101236.
[39] S.M.H. Zadeh, et al., Irreversibility analysis of thermally driven flow of a water-based suspension with dispersed nano-sized capsules of phase change material, Int. J. Heat Mass Transf. 155 (2020) 119796.
[40] S. Barlak, et al., Thermal conductivity and viscosity of nanofluids having nanoencapsulated phase change material, Nanosc. Microsc. Therm. Eng. 20 (2) (2016)

85–96.
[41] A. Rashad, et al., Entropy generation and MHD natural convection of a nanofluid in an inclined square porous cavity: effects of a heat sink and source size and location, Chin. J. Physics 56 (1) (2018) 193–211.
[42] A. Hajjar, S. Mehryan, M. Ghalambaz, Time periodic natural convection heat transfer in a nano-encapsulated phase-change suspension, Int. J. Mechanical Sci. 166 (2020) 105243.
[43] S.A.M. Mehryan, et al., Free convection in a trapezoidal enclosure divided by a flexible partition, Int. J. Heat Mass Transf. 149 (2020) 119186.
[44] B. Chen, et al., An experimental study of convective heat transfer with micro-encapsulated phase change material suspension: laminar flow in a circular tube under constant heat flux, Exp. Therm. Fluid Sci. 32 (8) (2008) 1638–1646.
[45] K. Khanafer, K. Vafai, A critical synthesis of thermophysical characteristics of nanofluids, Int. J. Heat Mass Transf. 54 (19–20) (2011) 4410–4428.
[46] F. Selimefendigil, H.F. Öztop, A.J. Chamkha, MHD mixed convection and entropy generation of nanofluid filled lid driven cavity under the influence of inclined magnetic fields imposed to its upper and lower diagonal triangular domains, J. Magn. Magn. Mater. 406 (2016) 266–281.
[47] M.H. Matin, I. Pop, Natural convection flow and heat transfer in an eccentric annulus filled by Copper nanofluid, Int. J. Heat Mass Transf. 61 (2013) 353–364.
[48] G. Cesini, et al., Natural convection from a horizontal cylinder in a rectangular cavity, Int. J. Heat Mass Transf. 42 (10) (1999) 1801–1811.
[49] G.G. Ilis, M. Mobedi, B. Sunden, Effect of aspect ratio on entropy generation in a rectangular cavity with differentially heated vertical walls, Int. Commun in Heat and Mass Transfer 35 (6) (2008) 696–703.